

Universal Persistent Brownian Motions in Confluent Tissues

Alessandro Rizzi and Sangwoo Kim*

Institute of Mechanical Engineering, École Polytechnique Fédérale de Lausanne (EPFL)

(Dated: February 26, 2026)

Biological tissues are active materials whose non-equilibrium dynamics emerge from distinct cellular force-generating mechanisms. Using a two-dimensional active foam model, we compare the effects of traction forces and junctional tension fluctuations on confluent tissue dynamics. While these two modes of activity produce qualitatively different cell shapes, rearrangement statistics, and spatiotemporal correlations in fluid states, we find that the long-time cellular motion universally converges to persistent Brownian dynamics. This universal feature contrasts with the non-universal correlations between cell geometry, rearrangement rate, and fluidity, which depend sensitively on the underlying modes of active force. Our results demonstrate that persistent Brownian motion provides a minimal framework for describing tissue dynamics, while distinct active forces leave identifiable structural and dynamical signatures, thereby enabling inference of the dominant active force in fluid state tissues.

Biological tissues are a prime example of active matter that constantly consumes energy at cellular and subcellular scales, driving dynamical changes in tissue architecture and mechanical states. This dynamic regulation plays a key role in many biological processes, including embryonic development, homeostasis, and disease progression [1, 2]. Although signaling pathways and gene expressions have been central in understanding these processes, recent studies highlight that modulating cellular mechanical properties is essential for robust control of tissue mechanical states.

In particular, accumulating studies show that biological tissues can induce phase transition behaviors between solid and fluid states through distinct mechanisms [3–6]. An increase in cell packing density within an epithelial monolayer exhibits glassy dynamics and caging behaviors [7], reminiscent of jamming and glass transition in soft materials [8, 9]. A confluent epithelial monolayer can also undergo phase transition by reaching a zero-tension state [10]. More recent studies show that phase transitions, including jamming, glass, and percolation transitions, play a key role in embryonic development across various organisms [11–15]. Complementing experimental observations, theoretical and computational models elucidate different modes of phase transitions, providing the physical basis for explaining such behaviors [14, 16–22].

While it is well established that increasing the magnitude of active forces leads to activity-induced phase transitions [19, 21, 23], how distinct modes of activity shape structural and dynamical features in non-equilibrium fluid states remains unclear. In this paper, we examine two well-known modes of active forces in densely packed monolayer systems, namely traction forces and junctional tension fluctuations, focusing on regimes in which one mode is dominant over the other, to identify similarities and differences in their emergent properties.

To that end, we employ a two-dimensional active foam model [21] under the confluent condition, i.e., with no spaces between cells. The geometry of individual cells

follows the vertex model framework, in which vertices at interfaces describe cell contours. In addition to the physical triple vertices at the tricellular junctions, intermediate vertices are introduced to capture complex cell shapes and junctional curvature (Fig. 1(a)). The tissue structure and dynamics follow from the vertex dynamics, described by an overdamped Langevin equation:

$$\eta_R \frac{d\mathbf{R}_\alpha}{dt} = \sum_{\langle i,j \rangle} \left[\mathbf{T}_{ij} \Theta(T_{ij}) + \mathbf{N}_{ij} \right] + \sum_k \mathbf{F}_k. \quad (1)$$

Here, \mathbf{R}_α denotes the position of vertex α , and \mathbf{T}_{ij} and \mathbf{N}_{ij} are the tangential and normal forces at the junc-

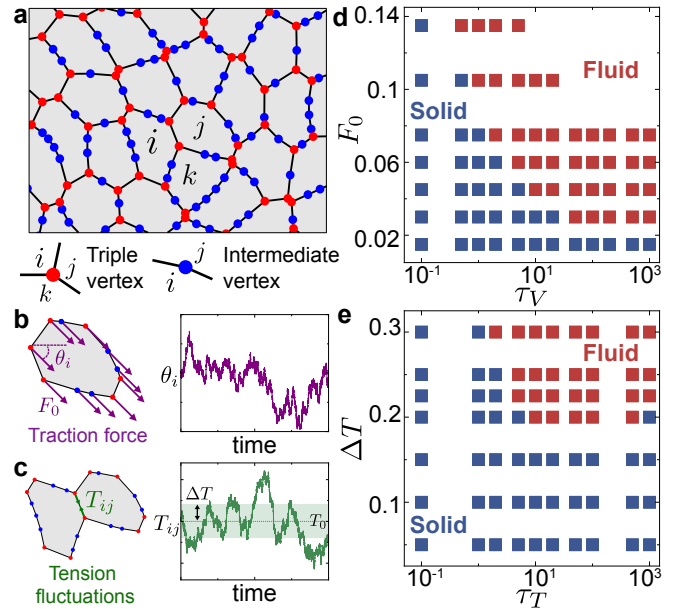


FIG. 1. Modeling framework and phase transition behaviors. (a) Representative tissue snapshot, showing distinct types of vertices. (b) Traction force as a self-propelling force, whose polarity θ_i diffuses over time. (c) Edge tension T_{ij} fluctuates around a fixed point T_0 . Phase diagram of (d) traction force, and (e) tension fluctuations, based on long-time MSRD.

tion between cell i and j associated with vertex α , and $\mathbf{F}_k = F_0 (\cos \theta_k, \sin \theta_k)$ is the traction force of cell k acting on vertex α . The effective force comprises three tangential, three normal, and three traction forces at a triple vertex, and two of each at an intermediate vertex (Fig. S7). The Heaviside step function $\Theta(T_{ij})$ prevents non-physical negative tension. The tangential force arises from the combined effects of cortical tension and cell-cell adhesion, setting a tension scale T_0 , while the normal force results from osmotic balance between cells. Note that the tangential and normal forces from standard vertex model energy functionals with area and perimeter elasticity can be mapped directly onto our formalism (see Supplementary Information, Section 2.3 and Fig. S8).

We consider two dominant modes of activity in isolation: traction forces and tension fluctuations. Cells generate traction force through focal adhesion, cytoskeletal reorganization, and actomyosin contractility [24, 25], which we model as a self-propulsion F_0 with polarity undergoing rotational diffusion as $\tau_V d\theta_i/dt = \xi$, where τ_V is the persistent timescale and ξ is the standard Gaussian noise of null mean and unit standard deviation, as in an active Brownian particle [26] (Fig. 1(b)). Although this force acts on the cell center, it can be equivalently represented as the same force acting on all vertices independent of intermediate vertices resolution, resulting in a constant speed F_0/η_R of an isolated cell, similar to traction implementation in previous studies [27–29].

Tension fluctuations arise from the dynamical regulation of the actomyosin cortex and cell-cell adhesion. We model these stochastic fluctuations using an Ornstein-Uhlenbeck process [20, 21, 30], in which the instantaneous tension fluctuates around the mean level T_0 by a fluctuation magnitude ΔT and a relaxation timescale τ_T (Fig. 1(c)).

$$\tau_T \frac{dT_{ij}}{dt} = -(T_{ij} - T_0) + \Delta T \sqrt{2\tau_T} \xi. \quad (2)$$

Both activities are characterized by two parameters, F_0 and τ_V for traction, and ΔT and τ_T for tension fluctuations. We will investigate these parameter pairs separately without mixing (i.e. $\Delta T = 0$ for traction and $F_0 = 0$ for tension fluctuations), while keeping other non-dimensional parameters fixed at biologically relevant scales (see SI, Section 2) Even for mixed cases, we confirm that our main results remain quantitatively unchanged when the characteristic scale of dominant active force is much larger than that of the others (see SI, Section 4 and Fig. S9).

We first investigate how the tissue mechanical states shift from solid to fluid under each mode of activity by computing the mean-squared relative displacement (MSRD); $MSRD(t) = \langle (\mathbf{r}_{ij}(t + t_0) - \mathbf{r}_{ij}(t_0))^2 \rangle$, where \mathbf{r}_{ij} is the displacement vector between cells i and j , which were neighbors at time t_0 . Both active forces drive a

transition from caging to subdiffusive and eventually diffusive behavior as activity increases, with superdiffusive exponents observed for traction forces at large F_0 and τ_V (Fig. S1(a)-(d)). We evaluate the MSRD at a fixed time, $t^* = 2500\tau_R$ (Fig. S1(e)(f)) and classify states as fluid when $MSRD(t^*) > 1$ (Fig. 1(d)(e)), which was shown to effectively distinguish solid and fluid states in non-equilibrium systems [11, 21]. Note that the specific choice of t^* only induces quantitative shifts in phase boundaries if t^* is larger than all other characteristic timescales in the system (Fig. S2).

Increasing the magnitude of activity, F_0 or ΔT , drives a transition from solid to fluid states, but the effect of the persistent timescale differs for the two modes. Increasing τ_V for traction monotonically fluidizes the system, whereas increasing τ_T for tension fluctuations induces a non-monotonic behavior in $MSRD(t^*)$, with maximal fluidity at intermediate persistence (Fig. 1(d)(e), Fig. S1(e)(f)). This contrast reflects intrinsic differences between the two modes. A large τ_V prolongs directed forces, enabling rearrangement even at lower F_0 . In contrast, both small and large τ_T hinder fluidization, as short τ_T does not provide sufficient persistence of junctional shortening, while long τ_T causes divergence between shortening and relaxation timescales.

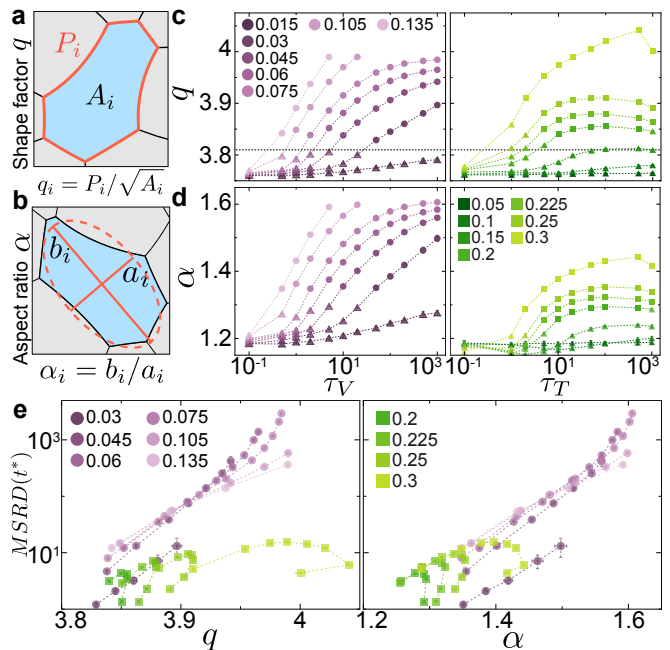


FIG. 2. Cell geometry in fluid states. Schematic representation of (a) shape factor q and (b) aspect ratio α . Cell anisotropy changes for traction (left) and tension fluctuations (right) in terms of (c) shape factor and (d) aspect ratio. The dashed line in (c) indicates $q_c = 3.81$. Triangles, circles, and squares respectively represent solid, fluid (traction), and fluid (tension fluctuations) states, as defined in Fig. 1(d)(e). (e) Correlations between shape factor, aspect ratio, and MSRD, exhibiting non-universal features.

The resulting phase diagrams agree with previous studies [19, 21, 31, 32], confirming that our model captures known non-equilibrium phase transitions driven by active forces. In the following, we will focus on fluid states to investigate how cell geometry, cellular rearrangements, and spatiotemporal correlations depend on the activity mode.

We first examine cell anisotropy, a key geometric signature of fluid states [17, 21], using two measures, the average shape factor $q = \langle q_i \rangle$ and aspect ratio $\alpha = \langle \alpha_i \rangle$. For each cell, the shape factor is defined as the ratio of the perimeter to the square root of area, $q_i = P_i / \sqrt{A_i}$ (Fig. 2(a)), and the aspect ratio is obtained by fitting an ellipse of major and minor axes b_i and a_i that preserves the eigenvalues of the second moment area, $\alpha_i = b_i / a_i$ (Fig. 2(b)).

For both traction and tension fluctuations, greater cell anisotropy correlates with increased motility and fluidity (Fig. 2(c-e)). For traction, the previously reported critical shape factor, $q_c \approx 3.81$ [17, 19], accurately predicts the solid-fluid boundary identified by $MSRD(t^*)$. However, the phase boundary prediction is less reliable for tension fluctuations, with solid states of $q > q_c$ at intermediate τ_T (Fig. 2(c)). The aspect ratio shows similar correlations, but its range is significantly narrower under tension fluctuations than under traction (Fig. 2(d)). These differences manifest as non-universal correlations between q and $MSRD(t^*)$, and between α and $MSRD(t^*)$ (Fig. 2(e)), implying that cell shape alone cannot robustly infer the level of fluidity, particularly in systems dominated by distinct active forces.

How cells deform from the isotropic shape also strongly depends on the type of activity. We compare representative cell geometries at fixed q under traction and tension fluctuations (Fig. 3(a)). At high q , cells under traction exhibit uniaxial elongation, whereas cells under tension

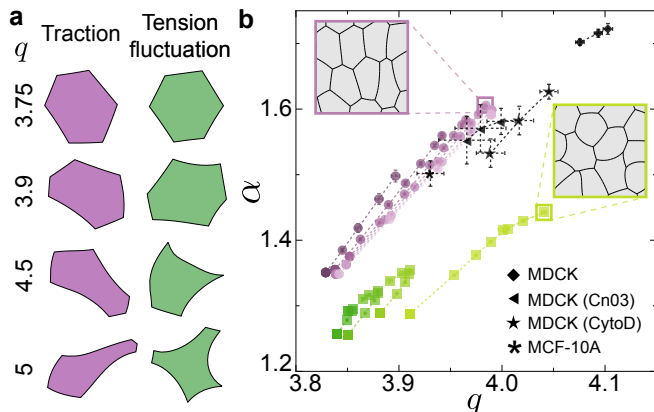


FIG. 3. Cell geometry in fluid states. (a) Representative cell shapes for distinct q . (b) Correlations between q and α for fluid states with experimental data [23, 33] shown as black markers. Error bars indicate the standard error of the mean. The insets illustrate the different morphologies at large q .

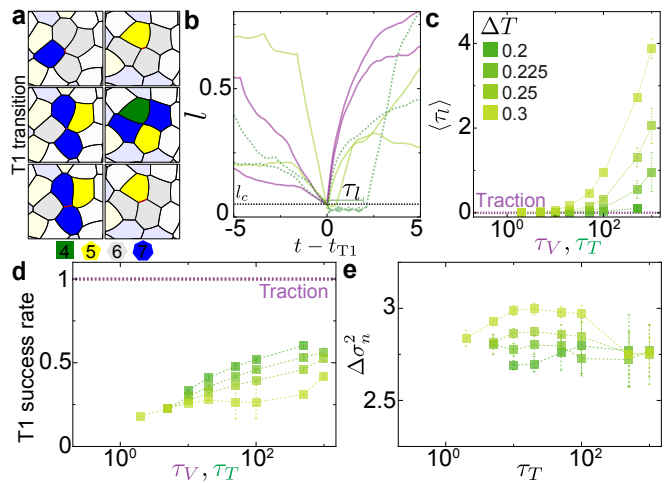


FIG. 4. T1 dynamics. (a) Schematics of a successful (left) and an unsuccessful (right) T1 transition. (b) Representative edge length evolution during a T1 transition for traction (purple) and tension fluctuations (green). Solid and dashed lines represent successful and unsuccessful T1 events, respectively. The gray line marks l_c . (c) Mean stalling time, and (d) T1 success rate for tension fluctuations. (e) Mean expected change in defect density for unsuccessful T1 transitions.

fluctuations develop highly curved long edges. While directed traction forces induce elongation and nematic order (Fig. S3), increasing tension fluctuations broaden the tension distribution, producing long, low-tension junctions with high curvature due to the Young-Laplace equation. Such lax junctions increase q without increasing cell elongation, yielding smaller aspect ratios at the same q (Fig. 3(b)).

To validate this, we analyze MDCK [33] and MCF-10A [23] monolayers in fluid states, where dominant activity is traction force (see SI, Section 5 and Fig. S10). MCF-10A and Cn03-treated MDCK cells match our simulations, while cytochalasin D-treated MDCK cells show reduced aspect ratios consistent with suppressed motility. Low-density MDCK cells fall outside of our simulation range but follow the same trend, confirming consistency with our results.

A similar non-universal feature appears in human bronchial epithelial layers undergoing either compression-induced unjamming or partial epithelial-to-mesenchymal transition (pEMT) [34], where lax junctions in the pEMT arise from reduced mean tension rather than fluctuations. Our results show that the same non-universal feature can emerge in non-equilibrium regimes.

We next analyze cellular rearrangements, an essential feature of fluidity. In confluent layers, these occur through T1 transitions, i.e., the loss of existing contacts and the formation of new junctions [35–38] (Fig. 4(a)). For both activities, higher fluidity corresponds to a higher T1 rate, θ_{T1} (Fig. S4). To characterize T1 dynamics, we track the length of each edge and identify $t = t_{T1}$ when

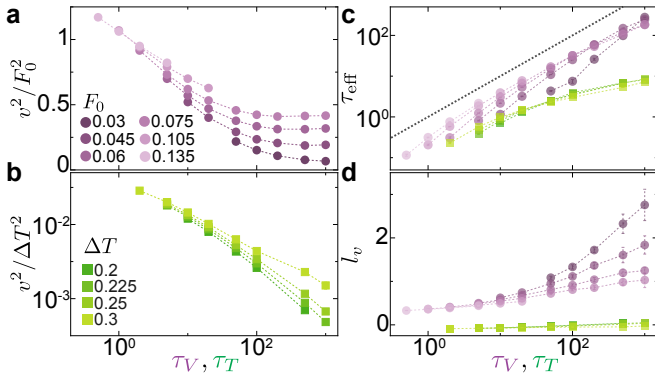


FIG. 5. Spatio-temporal correlations in cell dynamics. Normalized mean squared velocity for (a) traction (linear scale) and (b) tension fluctuations (log scale). (c) Effective persistence τ_{eff} and (d) correlation length l_v . The dashed line in (c) represents unity.

its length falls below the critical threshold l_c (Fig. 4(b), SI). Under traction, all short edges elongate immediately after the transition with zero stalling time $\tau_l = 0$. In contrast, under tension fluctuations, a fraction of edges exhibit finite stalling times, with both the stalled fraction (Fig. S5(b)(c)) and mean stalling time (Fig. 4(c), Fig. S5(d)) increasing with τ_T .

Beyond finite τ_l , the T1 success rate also differs qualitatively. We define a successful T1 as one that produces a net topology change (Fig. 4(a)). Under traction, the success rate is 1, whereas tension fluctuations produce a substantial fraction of unsuccessful events, reverting to the original topology (Fig. 4(a)(d)). This difference stems from force persistence; traction provides a persistent force throughout the rearrangement, whereas junctional shortening due to tension fluctuations loses directional memory after the transition. This result is consistent with previous studies with mechanical feedback [39].

An energy argument between adjacent local energy minima explains unsuccessful T1 transitions. Although the system is far from equilibrium, the underlying local energy minima and their energy level can be inferred from the defect density, $\sigma_n^2 = \langle (n_i - 6)^2 \rangle$, where n_i is the number of neighbors of cell i . In two-dimensional monodisperse systems, higher σ_n^2 corresponds to higher energy [40]. For unsuccessful T1 transitions, we compute the expected change in σ_n^2 assuming successful ones, $\Delta\sigma_n^2$, and find that they are biased toward energy-increasing configurations (Fig. 4(e)). In contrast, successful T1 transitions yield $|\Delta\sigma_n^2| \ll 1$, as required for steady states. Thus, energy landscape and local energy barriers strongly influence T1 dynamics under tension fluctuations, but not under traction forces.

Changes in the persistence of activity also affect cell velocity in distinct ways. Increasing persistence reduces the mean squared velocity, $v^2 = \langle v_i^2 \rangle$, in both cases, but traction reaches a constant speed, while tension fluctuations

slow down to zero (Fig. 5(a)(b)). The velocity plateau for traction arises from the balance between self-propulsion F_0 and passive force set by T_0 at large τ_V , similar to dense self-propelled particles [41]. On the other hand, large τ_T slows down junctional dynamics, solidifying tissue and reducing cell speed.

The spatial and temporal velocity correlations also show qualitative differences between the two activity modes. We compute temporal autocorrelation and spatial correlation functions, extracting an effective persistence time, τ_{eff} , and a velocity correlation length, l_v (see SI, Section 3). Increasing τ_V or τ_T enhances velocity persistence, though the effect is much weaker for tension fluctuations (Fig. 5(c), Fig. S6(a)(b)). While the inherent persistence for traction directly governs cell velocity, the persistence in tension fluctuations couples weakly to cell motion, making it less effective in increasing τ_{eff} . Furthermore, due to the sharp decrease in velocity, the persistent length of the single cell trajectory under tension fluctuations remains much smaller than a cell length even for large τ_{eff} (Fig. S6(c)). Under traction, collective motion spontaneously emerges with increasing τ_V , consistent with previous studies [42–45], while tension fluctuations consistently give $l_v \ll 1$, indicating the absence of collective motion (Fig. 5(d), Fig. S6(d)-(g), Supplementary movies 1-4).

Despite the clear differences in spatial and temporal correlations, long-time cellular movement can be universally described by persistent Brownian motion [46, 47]

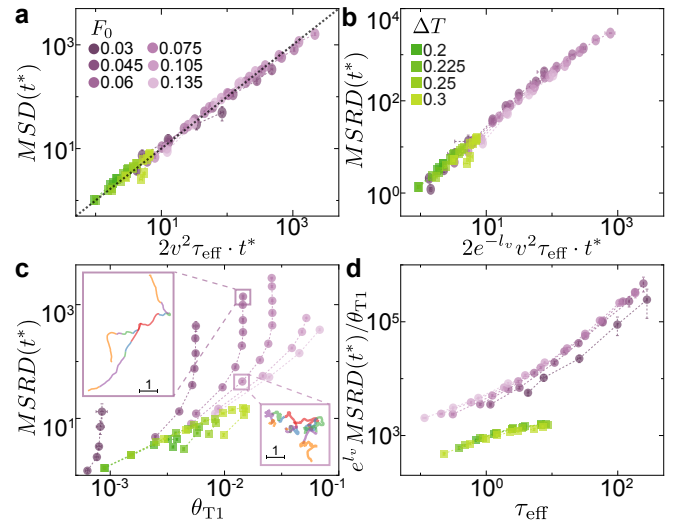


FIG. 6. Universal and non-universal correlations with cell movement. Long-time (a) MSD and (b) MSRDR can be predicted by persistent Brownian motion. (c) The MSRDR is not proportional to the T1 rate. The two insets show three cell trajectories over five T1 transitions with color changes for each T1 event. (d) MSRDR, corrected by l_v and scaled with θ_{T1} , collapses into two separate lines as a function of τ_{eff} . The dashed line in (a) represents unity.

$$MSD(t) = 2v^2\tau_{\text{eff}}^2 \left(t/\tau_{\text{eff}} - 1 + e^{-t/\tau_{\text{eff}}} \right). \quad (3)$$

The long-time limit of Eq. 3, $MSD(t^*) \approx 2v^2\tau_{\text{eff}} \cdot t^*$, predicts the MSD for both activities without free parameters (Fig. 6(a)). After correcting $MSRD$ by $e^{-t/\tau_{\text{eff}}}$, both activities collapse onto a single master curve (Fig. 6(b)), showing that long-time cellular movement is independent of the details of active forces.

In contrast, θ_{T1} does not reliably predict $MSRD(t^*)$ (Fig. 6(c)). This arises from the dependence of long-time cellular motion on persistence, as cells with higher persistence can separate by larger distances with the same number of T1 transitions (Fig. 6(c) insets, Supplementary movies 1-2). The long-time displacement per T1 rate correlates strongly with τ_{eff} , indicating that θ_{T1} alone cannot predict cellular movement, contrasting with recent studies reporting universal correlations [48, 49]. Even after accounting for τ_{eff} , the correlations split into two distinct branches, implying that additional non-equilibrium features, such as the typical traveling distance between T1 transitions, are required for a universal prediction.

In this work, we investigated non-equilibrium dynamics of confluent tissues under traction or tension fluctuations and showed that cell geometry, rearrangements, and spatiotemporal dynamics strongly depend on the specific mode of activity in fluid states. These differences lead to non-universal correlations with long-time cell movement, making it infeasible to predict $MSRD(t^*)$ from either cell shape or T1 rate. In contrast, $MSRD(t^*)$ is universally captured by persistent Brownian motion, consistent with prior observations in epithelial monolayers [47, 50, 51], suggesting a general description for biological tissues independent of active force details. Finally, the distinct structural and dynamical signatures between traction and tension fluctuations offer a potential method to infer the dominant active forces in tissues as an alternative approach to assess their mechanical states. Future work should explore mixed regimes with comparable active force magnitudes, together with other active processes such as cell division, apoptosis, extrusion, and insertion, to assess how universally the persistent Brownian dynamics framework can predict fluidity.

ACKNOWLEDGMENTS

The authors are grateful for helpful discussions with Sascha Hilgenfeldt, Cristina Marchetti, Adrien Méry, and Selman Sakar. We thank Scientific IT & Applications Support (SCITAS) for providing support with the high-performance computing facilities.

- [1] Charène Guillot and Thomas Lecuit. Mechanics of epithelial tissue homeostasis and morphogenesis. *Science*, 340(6137):1185–1189, 2013.
- [2] Carl-Philipp Heisenberg and Yohanns Bellaïche. Forces in tissue morphogenesis and patterning. *Cell*, 153(5):948–962, 2013.
- [3] Elizabeth Lawson-Keister and M Lisa Manning. Jamming and arrest of cell motion in biological tissues. *Current Opinion in Cell Biology*, 72:146–155, 2021.
- [4] Edouard Hannezo and Carl-Philipp Heisenberg. Rigidity transitions in development and disease. *Trends in Cell Biology*, 32(5):433–444, 2022.
- [5] Pierre-François Lenne and Vikas Trivedi. Sculpting tissues by phase transitions. *Nature Communications*, 13(1):664, 2022.
- [6] Yanlan Mao and Sara A Wickström. Mechanical state transitions in the regulation of tissue form and function. *Nature Reviews Molecular Cell Biology*, 25(8):654–670, 2024.
- [7] Thomas E. Angelini, Edouard Hannezo, Xavier Trepât, Manuel Marquez, Jeffrey J. Fredberg, and David A. Weitz. Glass-like dynamics of collective cell migration. *Proceedings of the National Academy of Sciences*, 108(12):4714–4719, 2011.
- [8] Corey S O’hern, Leonardo E Silbert, Andrea J Liu, and Sidney R Nagel. Jamming at zero temperature and zero applied stress: The epitome of disorder. *Physical Review E*, 68(1):011306, 2003.
- [9] M van Hecke. Jamming of soft particles: geometry, mechanics, scaling and isostaticity. *Journal of Physics: Condensed Matter*, 22(3):033101, 2010.
- [10] Jin-Ah Park, Jae Hun Kim, Dapeng Bi, Jennifer A Mitchel, Nader Taheri Qazvini, Kelan Tantisira, Chan Young Park, Maureen McGill, Sae-Hoon Kim, Bomi Gweon, et al. Unjamming and cell shape in the asthmatic airway epithelium. *Nature materials*, 14(10):1040–1048, 2015.
- [11] Alessandro Mongera, Payam Rowghanian, Hannah J Gustafson, Elijah Shelton, David A Kealhofer, Emmet K Carn, Friedhelm Serwane, Adam A Lucio, James Giammona, and Otger Campàs. A fluid-to-solid jamming transition underlies vertebrate body axis elongation. *Nature*, 561(7723):401–405, 2018.
- [12] Nicoletta I. Petridou, Silvia Grigolon, Guillaume Salbreux, Edouard Hannezo, and Carl-Philipp Heisenberg. Fluidization-mediated tissue spreading by mitotic cell rounding and non-canonical wnt signalling. *Nature Cell Biology*, 21(2):169–178, 2019.
- [13] Nicoletta I Petridou, Bernat Corominas-Murtra, Carl-Philipp Heisenberg, and Edouard Hannezo. Rigidity percolation uncovers a structural basis for embryonic tissue phase transitions. *Cell*, 184(7):1914–1928, 2021.
- [14] Sangwoo Kim, Rana Amini, Shuo-Ting Yen, Petr Pospíšil, Arthur Boutillon, Ilker Ali Deniz, and Otger Campàs. A nuclear jamming transition in vertebrate organogenesis. *Nature materials*, 23(11):1592–1599, 2024.
- [15] Tyler R. Huycke, Teemu J. Häkkinen, Hikaru Miyazaki, Vasudha Srivastava, Emilie Barruet, Christopher S. McGinnis, Ali Kalantari, Jake Cornwall-Scoones, Deepnya Vaka, Qin Zhu, Hyunil Jo, Roger Oria, Valerie M. Weaver, William F. DeGrado, Matt Thomson,

- Krishna Garikipati, Dario Boffelli, Ophir D. Klein, and Zev J. Gartner. Patterning and folding of intestinal villi by active mesenchymal dewetting. *Cell*, 187(12):3072–3089.e20, 2024.
- [16] Douglas B Staple, Reza Farhadifar, J-C Röper, Benoit Aigouy, Suzanne Eaton, and Frank Jülicher. Mechanics and remodelling of cell packings in epithelia. *The European Physical Journal E*, 33(2):117–127, 2010.
- [17] Dapeng Bi, JH Lopez, Jennifer M Schwarz, and M Lisa Manning. A density-independent rigidity transition in biological tissues. *Nature Physics*, 11(12):1074–1079, 2015.
- [18] Sangwoo Kim and Sascha Hilgenfeldt. Cell shapes and patterns as quantitative indicators of tissue stress in the plant epidermis. *Soft matter*, 11(37):7270–7275, 2015.
- [19] Dapeng Bi, Xingbo Yang, M Cristina Marchetti, and M Lisa Manning. Motility-driven glass and jamming transitions in biological tissues. *Physical Review X*, 6(2):021011, 2016.
- [20] Matej Krajnc. Solid–fluid transition and cell sorting in epithelia with junctional tension fluctuations. *Soft Matter*, 16(13):3209–3215, 2020.
- [21] Sangwoo Kim, Marie Pochitaloff, Georgina A Stooke-Vaughan, and Otger Campàs. Embryonic tissues as active foams. *Nature physics*, 17(7):859–866, 2021.
- [22] Zhu-Qin Li, Qun-Li Lei, and Yu-Qiang Ma. Fluidization and anomalous density fluctuations in 2d voronoi cell tissues with pulsating activity. *Proceedings of the National Academy of Sciences*, 122(10):e2421518122, 2025.
- [23] Chiara Malinverno, Salvatore Corallino, Fabio Giavazzi, Martin Bergert, Qingsen Li, Marco Leoni, Andrea Disanza, Emanuela Frittoli, Amanda Oldani, Emanuele Martini, Tobias Lendenmann, Gianluca De Florian, Galina V. Bezoussenko, Dimos Poulikakos, Kok Haur Ong, Marina Uroz, Xavier Trepát, Dario Parazzoli, Paolo Maiuri, Weimiao Yu, Aldo Ferrari, Roberto Cerbino, and Giorgio Scita. Endocytic reawakening of motility in jammed epithelia. *Nature Materials*, 16(5):587–596, 2017.
- [24] Agustí Brugués, Ester Anon, Vito Conte, Jim H Veldhuis, Mukund Gupta, Julien Colombelli, José J Muñoz, G Wayne Brodland, Benoit Ladoux, and Xavier Trepát. Forces driving epithelial wound healing. *Nature physics*, 10(9):683–690, 2014.
- [25] Ricard Alert and Xavier Trepát. Physical models of collective cell migration. *Annual Review of Condensed Matter Physics*, 11(1):77–101, 2020.
- [26] Pawel Romanczuk, Markus Bär, Werner Ebeling, Benjamin Lindner, and Lutz Schimansky-Geier. Active brownian particles: From individual to collective stochastic dynamics. *The European Physical Journal Special Topics*, 202(1):1–162, 2012.
- [27] Daniel M Sussman. cellgpu: Massively parallel simulations of dynamic vertex models. *Computer Physics Communications*, 219:400–406, 2017.
- [28] Souvik Sadhukhan, Manoj Kumar Nandi, Satyam Pandey, Matteo Paoluzzi, Chandan Dasgupta, Nir S Gov, and Saroj Kumar Nandi. Motility driven glassy dynamics in confluent epithelial monolayers. *Soft Matter*, 20(31):6160–6175, 2024.
- [29] Margherita De Marzio, Amit Das, Jeffrey J Fredberg, and Dapeng Bi. Epithelial layer fluidization by curvature-induced unjamming. *Physical review letters*, 134(13):138402, 2025.
- [30] Scott Curran, Charlotte Strandkvist, Jasper Bathmann, Marc De Gennes, Alexandre Kabla, Guillaume Salbreux, and Buzz Baum. Myosin ii controls junction fluctuations to guide epithelial tissue ordering. *Developmental cell*, 43(4):480–492, 2017.
- [31] Daniel L Barton, Silke Henkes, Cornelis J Weijer, and Rastko Sknepnek. Active vertex model for cell-resolution description of epithelial tissue mechanics. *PLoS computational biology*, 13(6):e1005569, 2017.
- [32] Takaki Yamamoto, Daniel M Sussman, Tatsuo Shibata, and M Lisa Manning. Non-monotonic fluidization generated by fluctuating edge tensions in confluent tissues. *Soft Matter*, 18(11):2168–2175, 2022.
- [33] Aashrith Saraswathibhatla, Emmett E Galles, and Jacob Notbohm. Spatiotemporal force and motion in collective cell migration. *Scientific Data*, 7(1):197, 2020.
- [34] Jennifer A Mitchel, Amit Das, Michael J O’Sullivan, Ian T Stancil, Stephen J DeCamp, Stephan Koehler, Oscar H Ocaña, James P Butler, Jeffrey J Fredberg, M Angela Nieto, et al. In primary airway epithelial cells, the unjamming transition is distinct from the epithelial-to-mesenchymal transition. *Nature communications*, 11(1):5053, 2020.
- [35] Elise Walck-Shannon and Jeff Hardin. Cell intercalation from top to bottom. *Nature reviews Molecular cell biology*, 15(1):34–48, 2014.
- [36] Dapeng Bi, Jorge H Lopez, Jennifer M Schwarz, and M Lisa Manning. Energy barriers and cell migration in densely packed tissues. *Soft matter*, 10(12):1885–1890, 2014.
- [37] Matej Krajnc, Sabyasachi Dasgupta, Primož Ziherl, and Jacques Prost. Fluidization of epithelial sheets by active cell rearrangements. *Physical Review E*, 98(2):022409, 2018.
- [38] Sangwoo Kim, Yiliang Wang, and Sascha Hilgenfeldt. Universal features of metastable state energies in cellular matter. *Physical review letters*, 120(24):248001, 2018.
- [39] Fernanda Pérez-Verdugo and Shiladitya Banerjee. Tension remodeling regulates topological transitions in epithelial tissues. *PRX life*, 1(2):023006, 2023.
- [40] Sangwoo Kim and Sascha Hilgenfeldt. A simple landscape of metastable state energies for two-dimensional cellular matter. *Soft Matter*, 15(2):237–242, 2019.
- [41] Grzegorz Szamel and Elijah Flenner. Extremely persistent dense active fluids. *Soft Matter*, 20(26):5237–5244, 2024.
- [42] Silke Henkes, Kaja Kostanjevec, J Martin Collinson, Rastko Sknepnek, and Eric Bertin. Dense active matter model of motion patterns in confluent cell monolayers. *Nature communications*, 11(1):1405, 2020.
- [43] Lorenzo Caprini, Umberto Marini Bettolo Marconi, and Andrea Puglisi. Spontaneous velocity alignment in motility-induced phase separation. *Physical review letters*, 124(7):078001, 2020.
- [44] Yann-Edwin Keta, Robert L Jack, and Ludovic Berthier. Disordered collective motion in dense assemblies of persistent particles. *Physical review letters*, 129(4):048002, 2022.
- [45] Meng-Yuan Li and Yan-Wei Li. Relaxation dynamics in the self-propelled voronoi model for epithelial monolayers. *Physical Review Research*, 6(3):033209, 2024.
- [46] Reinhold Fürth. Die brownsche bewegung bei berücksichtigung einer persistenz der bewegungsrichtung. mit anwendungen auf die bewegung lebender infusorien.

- Zeitschrift für Physik*, 2(3):244–256, 1920.
- [47] David Selmecki, Stephan Mosler, Peter H Hagedorn, Niels B Larsen, and Henrik Flyvbjerg. Cell motility as persistent random motion: theories from experiments. *Biophysical journal*, 89(2):912–931, 2005.
- [48] Harish P. Jain, Axel Voigt, and Luiza Angheluta. From cell intercalation to flow, the importance of t1 transitions. *Phys. Rev. Res.*, 6:033176, Aug 2024.
- [49] Harish P Jain, Richard DJG Ho, and Luiza Angheluta. Emergent cell migration from cell shape deformations and t1 transitions. *Physical Review Research*, 7(3):033020, 2025.
- [50] András Szabó, R Ünneper, Eld Méhes, WO Twaal, WS Argraves, Y Cao, and András Czirók. Collective cell motion in endothelial monolayers. *Physical biology*, 7(4):046007, 2010.
- [51] András Czirók, Katalin Varga, Előd Méhes, and András Szabó. Collective cell streams in epithelial monolayers depend on cell adhesion. *New journal of physics*, 15(7):075006, 2013.